Journal of Alloys and Compounds 884 (2021) 161022

Contents lists available at ScienceDirect

Journal of Alloys and Compounds

journal homepage: www.elsevier.com/locate/jalcom

Influence of vanadium concentration on up-conversion luminescence in Er^{3+}–Yb^{3+} and Tm^{3+}–Yb^{3+} ions pair co-doped $YV_xP_{1-x}O_4$ solid state solution

Marta Wujczyk, Adam Watras, Katarzyna Szyszka, Rafal J. Wiglusz*

Institute of Low Temperature and Structure Research, PAS, Okolna 2, 50-422 Wroclaw, Poland

ARTICLE INFO

Article history:
Received 25 February 2021
Received in revised form 28 June 2021
Accepted 29 June 2021
Available online 2 July 2021

Keywords:
Solid state solution
Yttrium orthovanadate
Yttrium orthophosphate
Lanthanide ions
Up-conversion

ABSTRACT

The paper is focused on an influence of vanadium ions on the up-conversion processes in nanosized $YV_xP_{1-x}O_4$ solid state solution. As a consequence, two series of $YV_xP_{1-x}O_4$ (where x = 0–1) materials has been obtained via co-precipitation method. Yttrium orthovanadate-phosphate has been co-doped with the up-converting Er^{3+}-Yb^{3+} and Tm^{3+}-Yb^{3+} lanthanide ion pairs. Obtained series of nanosized materials has been investigated for phase purity, chemical composition, morphology by the means of X-Ray Powder Diffraction (XRD) and Scanning Electron Microscope (SEM). Photoluminescence properties of 0.25 mol% Tm^{3+}, 20 mol% Yb^{3+}:$YV_xP_{1-x}O_4$ (x = 0, 0.3, 0.4, 0.5, 0.6, 0.7, 1), and 1 mol% Er^{3+}, 20 mol% Yb^{3+}:$YV_xP_{1-x}O_4$ (x = 0, 0.3, 0.4, 0.5, 0.6, 0.7, 1) were investigated in detail. It has been found that increase of the vanadium content leading to better up-conversion luminescence.

1. Introduction

Recently, rare earth doped and co-doped yttrium orthooxides have attracted an astonishing interest and have been investigated as phosphors for UV, Vis, and NIR excitations. The interest of YXO_4 (where X = As, Cr, P, V) is related to physicochemical properties such as high-temperature stability, resistivity to photo degradation, insolubility in water [1]. Among the extensive studies of the YXO_4 matrices it was also investigated for occurrence of up- and down-conversion processes [2–10]. Although, to the best of our knowledge up-conversion processes in the mixed $YV_xP_{1-x}O_4$ solid solutions have not been investigated.

Yttrium orthovanadate as well as yttrium orthophosphate crystallize in the tetragonal system and are ascribed by $I4_1/amd$ space group [11,12]. Moreover, yttrium orthovanadate is isostructural to yttrium orthophosphate. Therefore, a solid-state solution with general formula YVxP1-xO4 may be obtained. The unit cell is built out of the yttrium octahedral and vanadium tetrahedral, which is statistically substituted by phosphorus tetrahedral groups. Yttrium ions are also substituted in a statistical manner, when doped or co-doped with lanthanide ions (i.e., Tm^{3+}, Er^{3+} and Yb^{3+} ions).

Up-conversion (UC) processes are based on the energy conversion from low energy (IR, NIR) to the higher energy (UV, Vis). F. Auzel [13] has compartmentalized UC processes into six different processes: ESA (Excited State Absorption), APTE/ETU (Addition de Photon par Transfers d'Energie/Energy Transfer Up-conversion), cooperative sensitization, cooperative luminescence, second harmonic generation (SHG) and 2-photon absorption excitation. Although, the quantum efficiency (QE) of the up-conversion processes is relatively low, ETU and ESA processes present highest quantum efficiency out of the mentioned processes [13].

This paper is focused on an investigation of the up-conversion processes that are influenced by concentration of vanadium ions in $YV_xP_{1-x}O_4$ matrix. The concentration of the vanadium ions is in the range of $0 \le x \le 1$ in respect to the appropriate phosphorus molar content. Moreover, two pairs of co-dopants related to Tm^{3+}-Yb^{3+} and Er^{3+}-Yb^{3+} ions were used. In both cases, 20 mol% Yb^{3+} ion was chosen as a sensitizer and 0.25 mol% Tm^{3+} as well as 1 mol% Er^{3+} ions were chosen as activators. The series of 0.25 mol% Tm^{3+}, 20 mol% Yb^{3+}:$YV_xP_{1-x}O_4$ (where x = 0, 0.3, 0.4, 0.5, 0.6, 0.7, 1) and 1 mol% Er^{3+}, 20 mol% Yb^{3+}:$YV_xP_{1-x}O_4$ (where x = 0, 0.3, 0.4, 0.5, 0.6, 0.7, 1) samples were obtained via co-precipitation synthesis method and thereafter heat-treated at 800 °C for 3 h.

* Corresponding author.
E-mail address: r.wiglusz@intibs.pl (R.J. Wiglusz).

https://doi.org/10.1016/j.jallcom.2021.161022
0925-8388/

Table 1
Crystallographic data for yttrium orthovanadate and yttrium orthophosphate [14,15].

	YVO_4	YPO_4
cryst. syst.	zircon tetragonal	zircon tetragonal
space group	$I4_1/amd$ (no.141)	$I4_1/amd$ (no.141)
a **(Å)**	7.1183(1)	6.8947(6)
b **(Å)**	7.1183(1)	6.8947(6)
c **(Å)**	6.2893(1)	6.0276(6)
α (°)	90	90
β (°)	90	90
γ (°)	90	90
point-group symmetry	D_{4h}	D_{4h}
coordination no.	Y(8); V(4); O(3)	Y(8); P(4); O(3)

2. Experimental

2.1. Synthesis

Nano-sized yttrium orthovanadate-phosphate doped with ytterbium-thulium and ytterbium-erbium ions were prepared by wet chemical synthesis via co-precipitation method. Concentration of the optically active ions was set to 0.25 mol% Tm^{3+}, 20 mol% Yb^{3+} and 1 mol% Er^{3+}, 20 mol% Yb^{3+} for each material, in respect to the appropriate Y^{3+} molar content. The V^{5+} ions concentration was changed from 30 to 70 mol%, respective to the appropriate P^{5+} molar content. Analytical grade Y_2O_3 (99.99% Alfa Aesar), Tm_2O_3 (99.99% Alfa Aesar), Yb_2O_3 (99.99% Alfa Aesar), Er_2O_3 (99.99% Alfa Aesar), $(NH_4)_2HPO_4$ (> 98% ACROS Organics) and NH_4VO_3 (99.5% Sigma-Aldrich) were used as the starting materials.

In this method, stoichiometric amounts of the lanthanide oxides were digested in an excess of 65% HNO_3 (about 2 ml; Suprapur® Merck) to transform them into nitrate salts. The obtained lanthanide nitrates were re-crystallized three times to get rid of the HNO_3 excess. Ammonium metavanadate and diammonium phosphate were dissolved in deionized water separately. Next, $(NH_4)_2HPO_4$ and NH_4VO_3 solutions were mixed and thereafter nitrate salts solution was added ($Y(NO_3)_3$, $Tm(NO_3)_3$, $Yb(NO_3)_3$ and $Y(NO_3)_3$, $Er(NO_3)_3$, $Yb(NO_3)_3$). Reaction (about 150 ml) was maintained at a stirring plate for 1.5 h at approximately 70 °C. The pH of the suspension was adjusted to 9 with aqueous ammonia (25% Avantor Poland). The obtained precipitate was washed and centrifuged at least thrice to reach neutral pH value. The as-prepared materials were dried for 24 h at 70 °C and heat-treated at 800 °C for 3 h to form crystallized nanoparticles.

2.2. XRD and SEM analysis

The development of the crystal phase was analysed via X-ray diffraction (XRD). The diffractograms were collected with an X'Pert PRO X-ray diffractometer (Cu Kα1, 1.54060 Å) (PANalytical). The XRD patterns were assigned to standard patterns from Inorganic Crystal Structure Database (ICSD) and thereafter analysed. Analysis of the size and morphology, as well as dispersibility of the $YV_xP_{1-x}O_4$ was performed on the SEM (Scanning Electron Microscope) FEI Nova NanoSEM 230 equipped with an EDS spectrometer (EDAX Genesis XM4).

2.3. Spectroscopic analysis

Emission spectra were recorded upon 980 nm excitation with diode laser (CW) at 300 K. A Schott KG5 and THORLABS FESH0850 were used as filters. For the measurements of up-conversion emission of 1 mol% Er^{3+}, 20 mol% Yb^{3+}: $YV_xP_{1-x}O_4$ only THORLABS FESH0850 filter was used. Two filters were used for up-conversion emission of 0.25 mol% Tm^{3+}, 20 mol% Yb^{3+}: $YV_xP_{1-x}O_4$. THORLABS FESH0850 filter does not fully transmit in 450 – 500 nm spectral region. Schott KG5 filter transmits in 450 – 500 nm but not in 600 – 800 spectral regions. Therefore, the presented emission spectra of 0.25 mol% Tm^{3+}, 20 mol% Yb^{3+}: $YV_xP_{1-x}O_4$ are compiled from two measurements preformed on the same setup, varying only on applied filter. The Hamamatsu PMA-12 photonic multichannel analyser was used as an optical detector. Power dependence of the up-conversion emission intensity was performed for a wide range of laser pump power 0.05–1.4 W, while excited upon 980 nm at 300 K. Data was fitted in respect to the following formula:

$$N_i \sim P^n, \quad (1)$$

where P – absorbed pump power, n – number of sequentially absorbed photons, N – population density of i state.

3. Results and discussion

3.1. Structure and morphology

The crystal structure of YXO_4 (where X = P, V) group of compounds is tetragonal with space group $I4_1/amd$ (No. 141), with only one cationic site for yttrium, which is substituted by rare earth ions

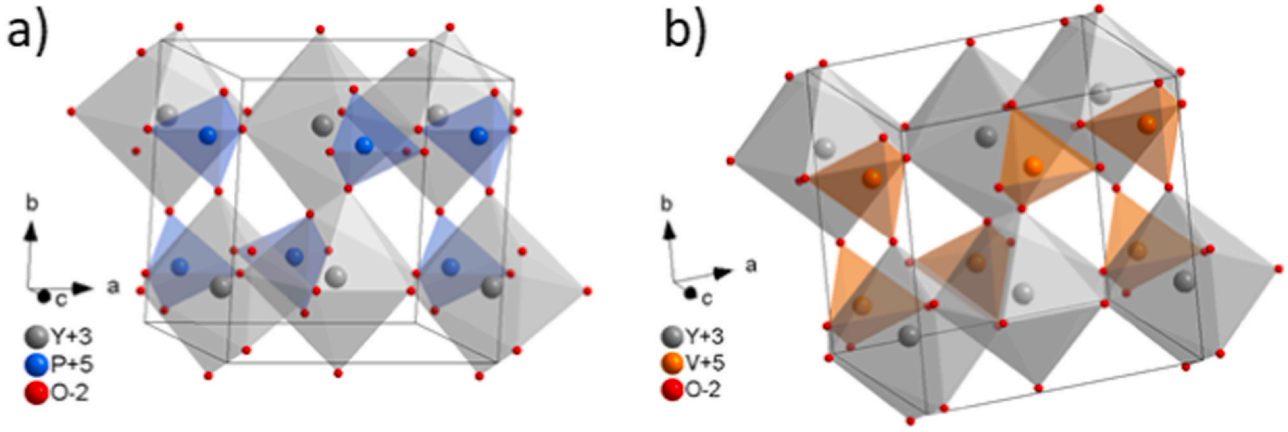

Fig. 1. 3D view of the YPO_4 (a) and YVO_4 (b) unit cells.

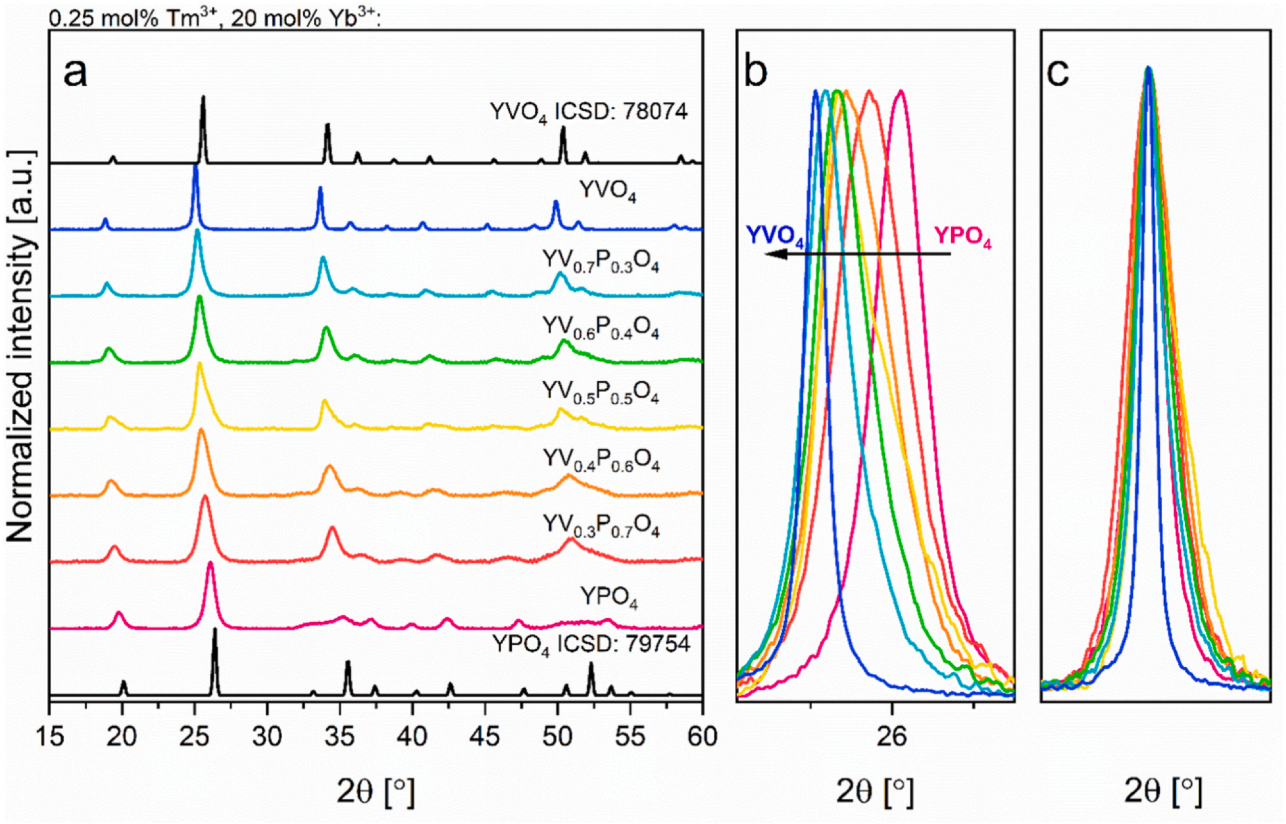

Fig. 2. X-ray diffraction patterns (a), 2theta shift (b) and (c) centered peak for bandwidth analysis, obtained for 0.25 mol% Tm^{3+}, 20 mol% Yb^{3+}:$YV_xP_{1-x}O_4$ thermally treated at 800 °C for 3 h.

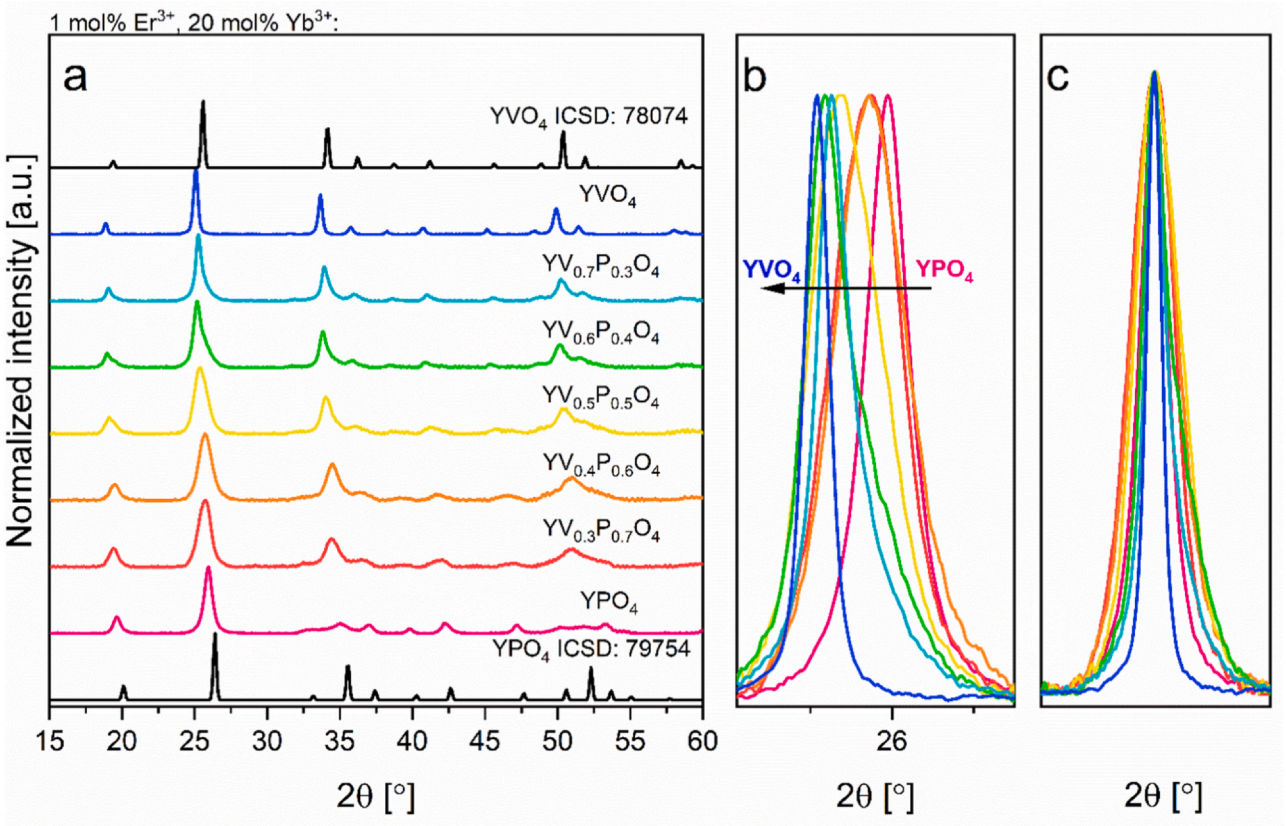

Fig. 3. X-ray diffraction patterns (a), 2θ shifts (b) and (c) centered peak for bandwidth analysis, obtained for 1 mol% Er^{3+}, 20 mol% Yb^{3+}:$YV_xP_{1-x}O_4$ thermally treated at 800 °C for 3 h.

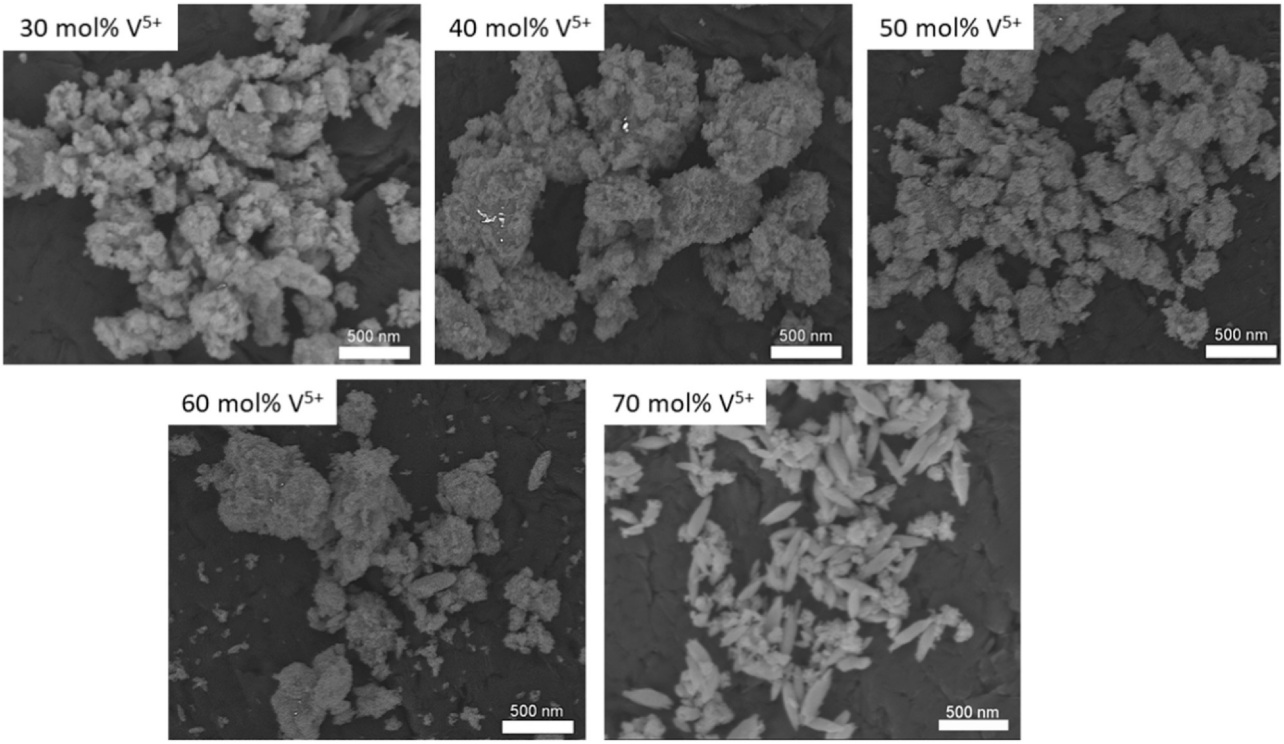

Fig. 4. SEM images obtained for 1 mol% Er^{3+}, 20 mol% Yb^{3+}:$YV_xP_{1-x}O_4$ thermally treated at 800 °C for 3 h.

(Tm^{3+}, Er^{3+}, Yb^{3+}). Unit cell parameters of the YVO_4 and YPO_4 are listed in Table 1.

As it was already presented in the case of $YV_xP_{1-x}O_4$ and Eu^{3+}:$YV_xP_{1-x}O_4$ obtaining the solid solution via co-precipitation method is possible [16,17]. Therefore, the $YV_xP_{1-x}O_4$ system co-doped with up-converting ions (Tm^{3+}, Er^{3+}, Yb^{3+}) should also be in accordance with the Vegard's law for solid solutions.(Fig. 1).

The formation of pure crystal phase of $YV_xP_{1-x}O_4$ solid solution was affirmed by the means of X-ray powder diffraction measurements (see Fig. 2 and 3). Crystal phase purity was obtained for the heat-treated materials differing in vanadium to phosphor ratio and in co-dopants (0.25 mol% Tm^{3+}, 20 mol% Yb^{3+} and 1 mol% Er^{3+}, 20 mol% Yb^{3+}). A continuous shift of the planes towards lower 2θ angles was observed and this is a confirmation of the unit cell parameters change. The change is forced by the substitution of the bigger V^{5+} (0.36 Å at C.N. 4) cation by smaller one P^{5+} (0.17 Å at C.N. 4) (**see** Fig. 2**b** and **3b**). Diffraction line broadening is observed for the solid solutions, when compared to the YPO_4 and YVO_4 matrices obtained at the equivalent synthesis conditions (**see** Fig. 2**c** and 3**c**). Broadening of the diffraction lines can possibly be a consequence of the lattice strain in the crystal lattice [18] and P^{5+} ions are substituted by V^{5+} ions. The strain may originate from the ionic size incompatibility between V^{5+} and P^{5+} ions. The lattice strain can be associated with the grain-interior dislocations [19], grain-boundary dislocations [20] and excess volume of grain boundaries (vacancies, vacancy clusters) [21]. Similar broadening of the XRD lines for $YV_xP_{1-x}O_4$ solid solution was observed by Nguyen H.D. et al. [22], were investigated materials were doped with bismuth and europium ions. Therefore it may be concluded that, the change of the

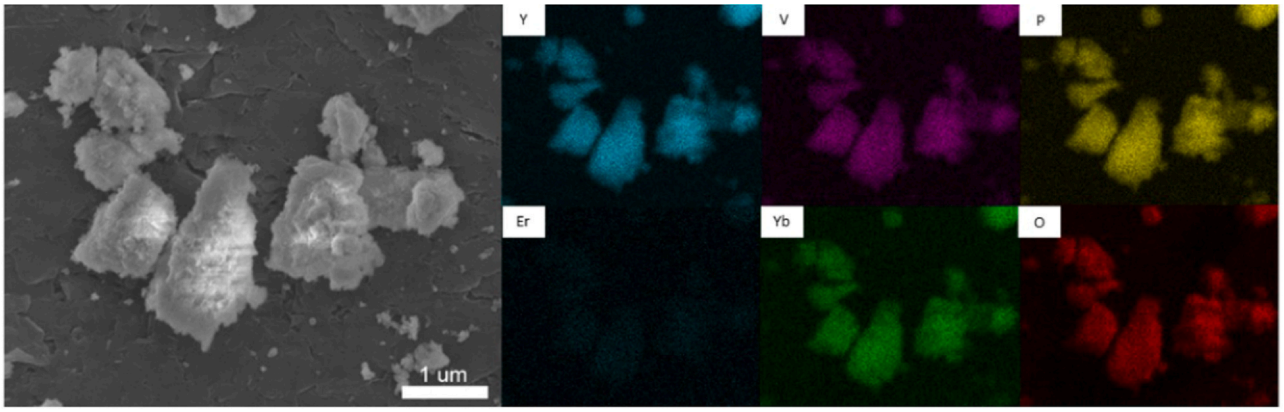

Fig. 5. EDS maps obtained for 1 mol% Er^{3+}, 20 mol% Yb^{3+}:$YV_{0.5}P_{0.5}O_4$ thermally treated at 800 °C for 3 h.

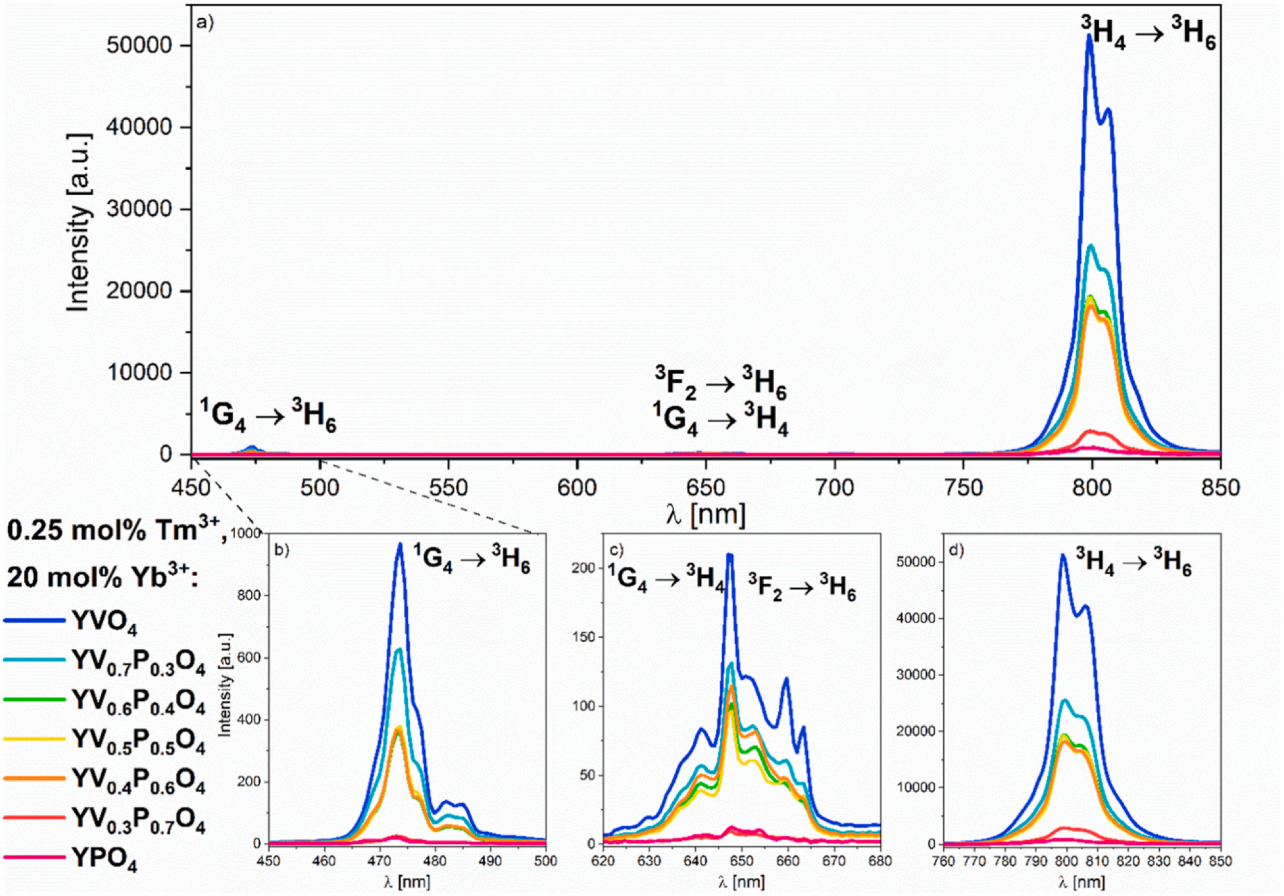

Fig. 6. Emission spectra of 0.25 mol% Tm^{3+}, 20 mol% Yb^{3+}:$YV_xP_{1-x}O_4$ under 980 nm excitation in room temperature.

diffraction lines width is not dependent on co-doping ions, but rather on the ionic radii mismatch between P^{5+} and V^{5+}.

SEM images are presented for the representative 0.25 mol% Tm^{3+}, 20 mol% Yb^{3+}:$YV_xP_{1-x}O_4$ material series, each thermally treated at 800 °C for 3 h (Fig. 4). Materials with low vanadium concentration have smaller and more agglomerated particles. On the contrary, the material with highest vanadium concentration presents less agglomerated and bigger particles with pellet or spindle like morphology. EDS maps (Fig. 5) present distribution of the ions in the representative 0.25 mol% Tm^{3+}, 20 mol% Yb^{3+}:$YV_{0.5}P_{0.5}O_4$ material's particles. Constituents are distributed evenly in the matrix structure and no conspicuous aggregation of the dopants is observed.

3.2. Spectroscopic properties

Up-conversion emission spectra of the 0.25 mol% Tm^{3+}, 20 mol% Yb^{3+}:$YV_xP_{1-x}O_4$ and 1 mol% Er^{3+}, 20 mol% Yb^{3+}:$YV_xP_{1-x}O_4$ are shown in Fig. 6 and Fig. 7, respectively. Emission spectra obtained for the materials containing Tm^{3+} and Yb^{3+} ions present visible transitions at around 473 nm, 645 nm, 660 nm and 800 nm, ascribed as the $^1G_4 \rightarrow {}^3H_6$, $^1G_4 \rightarrow {}^3H_4$, $^3F_2 \rightarrow {}^3H_6$, $^3H_4 \rightarrow {}^3H_6$ Tm^{3+} *f-f* transitions, respectively. The material with the highest emission intensity is 0.25 mol% Tm^{3+}, 20 mol% Yb^{3+}:YVO_4 and the material with the weakest is 0.25 mol% Tm^{3+}, 20 mol% Yb^{3+}:YPO_4. Intensity of the emission steadily increases with the increase of vanadium ions concentration in materials. No change in the shape of the transition bands was observed. No additional emission was recorded. No other evident influence of vanadium was observed than the emission intensity enhancement when introduced to the YPO_4 matrix.

Up-conversion emission spectra obtained for the 1 mol% Er^{3+}, 20 mol% Yb^{3+} material series, while excited under 980 nm at 300 K, present characteristic emission lines of erbium ions. The emission lines observed at 525 and 547 nm are attributed to the $^2H_{11/2} \rightarrow {}^4I_{15/2}$ and $^4S_{3/2} \rightarrow {}^4I_{15/2}$ transitions of Er^{3+} ions (sensitizer), respectively. Emission at around 650 nm is assigned to the $^4F_{9/2} \rightarrow {}^4I_{15/2}$ transition. Emission observed at 820 nm, 830 nm and 849 nm is associated with the $^4F_{7/2} \rightarrow {}^4I_{11/2}$, $^2H_{9/2} \rightarrow {}^4I_{11/2}$ and $^2H_{11/2} \rightarrow {}^4I_{13/2}$ transitions within erbium ions. Intensity of the emission simultaneously increases with the increase of vanadium ions concentration in materials. Additionally, the share of the respective transition bands changes in reference to the total emission, this relation is presented in Fig. 8.

With an increase of vanadium concentration in solid solution, a contribution of the $^4F_{9/2} \rightarrow {}^4I_{15/2}$ transition band decreases in favor of both the $^2H_{11/2} \rightarrow {}^4I_{15/2}$ and $^4S_{3/2} \rightarrow {}^4I_{15/2}$ transition bands (see Fig. 8). Additionally, solid solutions differ in emission band shapes. The difference is prominent in materials with marginal values of the

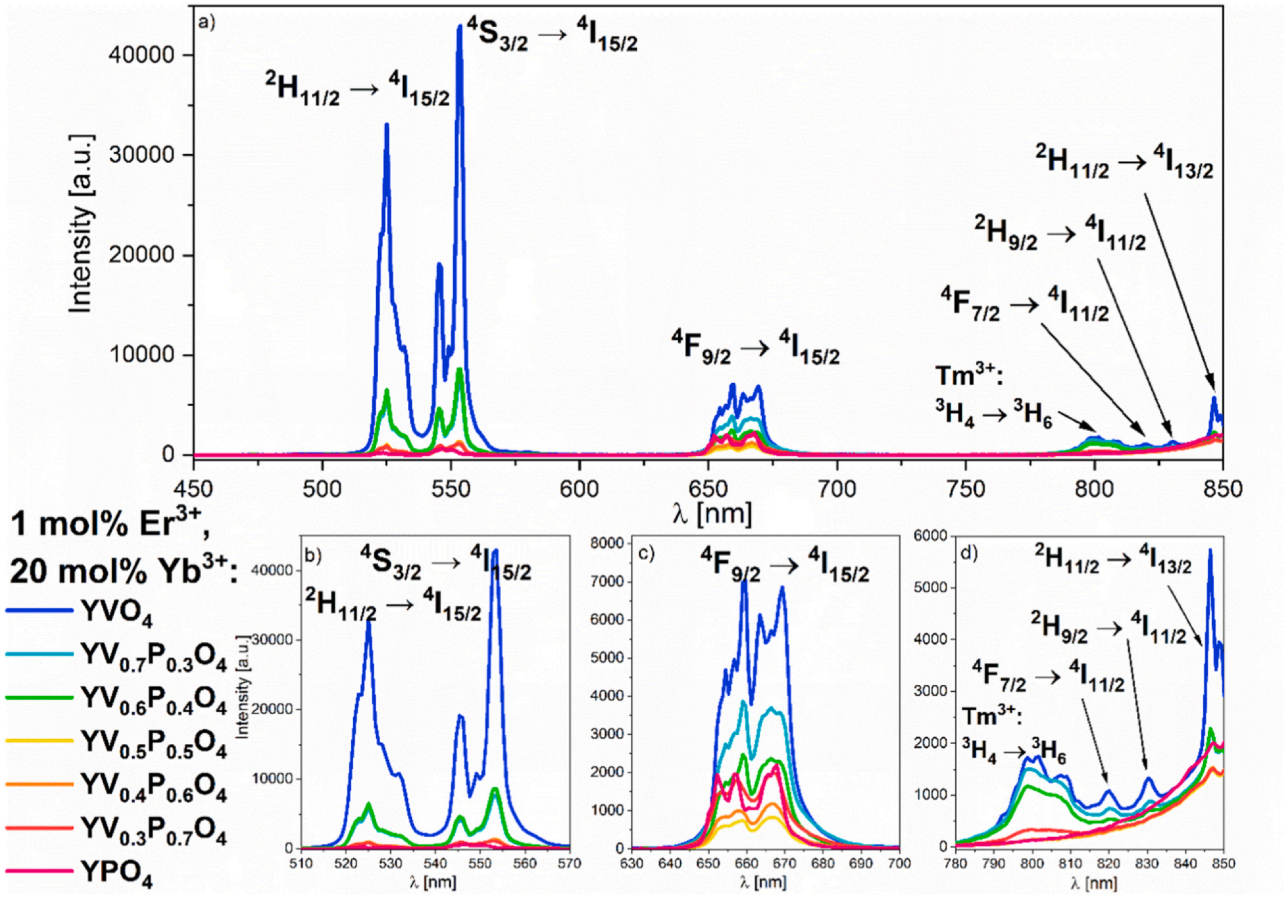

Fig. 7. Emission spectra of 1 mol% Er^{3+}, 20 mol% Yb^{3+}:$YV_xP_{1-x}O_4$ under 980 nm excitation at room temperature.

vanadium concentration (30 mol% V^{5+} and 70 mol% V^{5+}). The $^4F_{9/2} \rightarrow {}^4I_{15/2}$ transition contribution changing with increasing P^{5+} concentration may be caused by the occurring cross-relaxation (CR) processes. Population of the $^4F_{9/2}$ level is directly corelated with CR processes and its happening is dependent on the distance between two adjacent Er^{3+} ions in crystal lattice. In case of $YV_xP_{1-x}O_4$ the unit cell size visibly changes, where YPO_4 unit cell size being much smaller than YVO_4 due to different ionic radii of P^{5+} and V^{5+}. Therefore, the distance between two Er^{3+} ions in material containing low concentration of vanadium is shorter, hence it may be direct cause behind the increase in the intensity of the $^4F_{9/2} \rightarrow {}^4I_{15/2}$ transition.

The intensity of the up-conversion process increases with the increase of vanadium ions concentration in both Er/Yb and Tm/Yb co-doped materials. This means that vanadium ions have positive impact on emission intensity, independently on the used pairs of upconverting ions in this material. Moreover, the shape of particular transitions as well as the ratio of particular transition is influenced by vanadium ions concentration and is much more visible in case of Er/Yb ions pair.

A double logarithmic dependence of the integrated intensity versus laser pump power was investigated for each up-converting ions pair (Figs. 9, 10). Measurements were performed in a wide range of the laser pump power 0.05 – 1.43 W. Power dependence (PD) functions were determined for the $^2H_{11/2}$, $^4S_{3/2}$, $^4F_{9/2} \rightarrow {}^4I_{15/2}$ transitions and for the $^1G_4$, $^3H_4 \rightarrow {}^3H_6$ transitions for each material. According to the equations described by M. Pollnau (Eq. 1), the amount of photons needed for the up-conversion process can be estimated from the slope of the PD function [23]. Estimated number of photons is marked with the symbol *n* and is listed in inserted table in Figs. 9 and 10 for every material. Linear nature of the power dependence's function slope is reaffirming domination of the up-conversion processes over the linear decay from the indirect excited states. The 1 mol% Er^{3+}, 20 mol% Yb^{3+}:$YV_xP_{1-x}O_4$ (Fig. 9) independently on the vanadium concentration yielded *n* value equal to 2. Therefore, the two-photon nature behind population of the $^4F_{9/2}$, $^2H_{11/2}$ and $^4S_{3/2}$ states is confirmed. The 0.25 mol% Tm^{3+}, 20 mol% Yb^{3+}:$YV_xP_{1-x}O_4$ (Fig. 10) independently on the vanadium concentration yielded *n* value equal to 2 for the $^1G_4 \rightarrow {}^3H_6$ and $^3H_4 \rightarrow {}^3H_6$ transitions. Based on power dependence functions presented in Fig. 10b, it can be

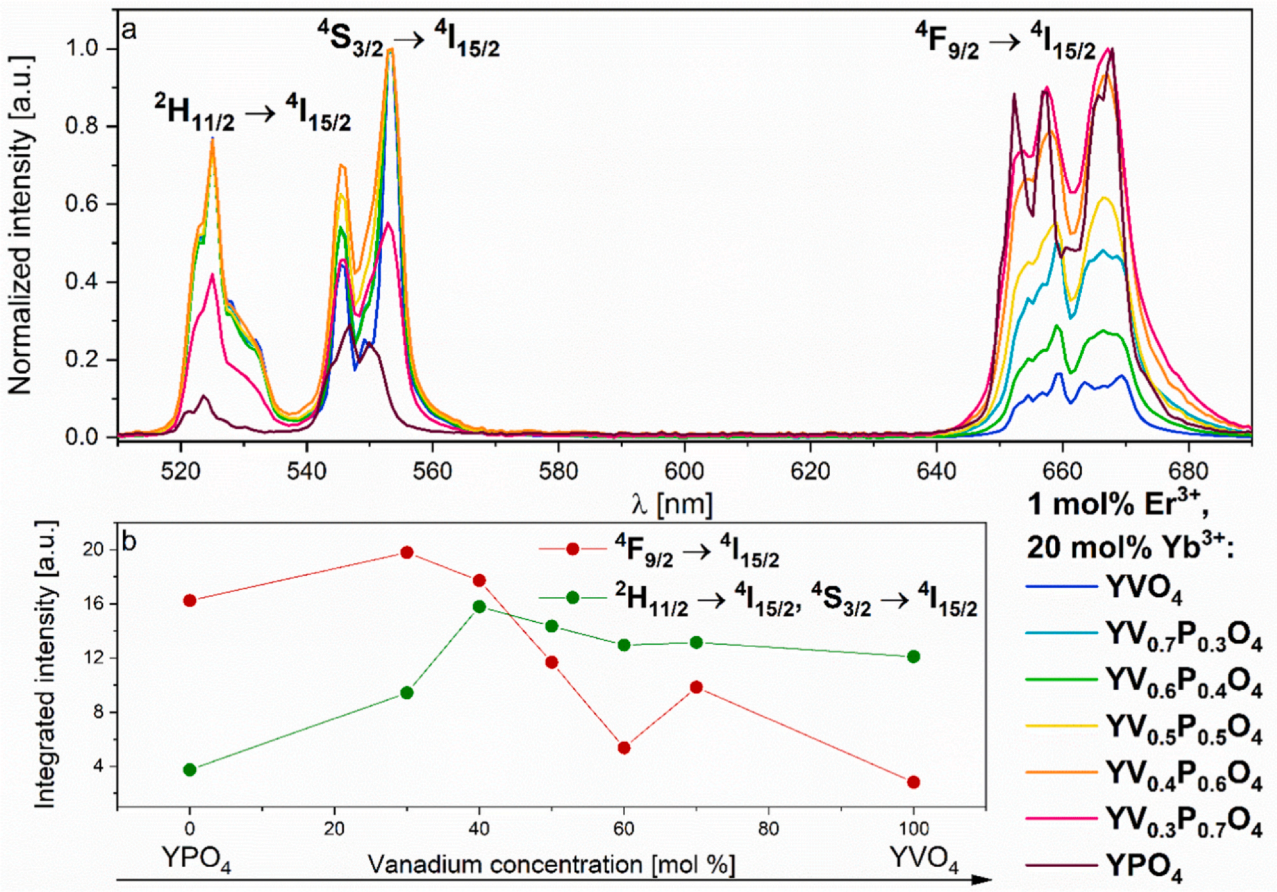

Fig. 8. Emission spectra of 1 mol% Er^{3+}, 20 mol% Yb^{3+}:$YV_xP_{1-x}O_4$ with normalized emission intensity (a) and of the integrated emission intensity dependence on vanadium concentration (b).

suggested that population of the $^1G_4$ state involves absorption of the two subsequent photons. Although, in order to populate the $^1G_4$ state, three photons need to be subsequently absorbed, when excited under 980 nm [24]. Decrease of the *n* value to 2 can be explained by the increase of the energy transfer rate from the sensitizer Yb^{3+} to the activator Tm^{3+} and additional contribution of the cooperative sensitization process to populate $^1G_4$, via Yb^{3+}-Yb^{3+} to Tm^{3+} energy transfer [25,26]. Possible pathways for the population of the $^1G_4$ state are given in Fig. 10.

The energy levels schemes in Fig. 11 and Fig. 12 shows the proposed model pathway for up-conversion processes occurring between Tm^{3+}-Yb^{3+} and Er^{3+}-Yb^{3+} ions in $YV_xP_{1-x}O_4$ solid state solution. Proposed pathways concern a series of $YV_xP_{1-x}O_4$ materials due to the fact related to emission spectra (Figs. 6 and 7) only vary in respective intensities and no additional *f-f* transition bands are found. Excitation wavelength is directly resonant with the sensitizer's (Yb^{3+}) large absorption cross section, its energy can be transferred to the activators (Tm^{3+}, Er^{3+}) with ease [27–29].

Within materials co-doped with 0.25 mol% Tm^{3+} and 20 mol% Yb^{3+} the process proceeding the ETU is Ground State Absorption (GSA), marked with black, solid arrow in the Fig. 11**.** Energy Transfer Up-conversion (ETU) process between the sensitizer (Yb^{3+}) and the acceptors (Er^{3+} and Tm^{3+}) is marked with black, bended arrows insinuating energy transfer from the sensitizer to the acceptors. Population of the Tm^{3+} upper levels is preceded by energy transfer from Yb^{3+} ions in the thulium-ytterbium co-doped materials. Although, the population of the $^3F_4$ level is more complex. The $^3F_4$ level can be populated via two possible pathways by the non-resonant ground state absorption of initial light (black, solid arrow), followed by non-radiative relaxation to the $^3H_5$, further depopulated to the $^3F_4$. Additionally, the $^3F_4$ is populated by the non-resonant energy transfer (black, bended arrow) from the pumped $^2F_{5/2}$ level in Yb^{3+} ion to the $^3H_5$ state in Tm^{3+} ion and later, depopulated to the $^3F_4$. Further, the $^3F_2$ state is populated by the non-resonant energy transfer from the $^2F_{5/2}$ level (Yb^{3+}), then followed by emission to the ground state ($^3F_2 \rightarrow {}^3H_6$ at 660 nm) or by non-radiative relaxation to the $^3H_4$. After that emission may be observed at 798 nm ($^3H_4 \rightarrow {}^3H_6$). Subsequently, the $^1G_4$ level may also be populated by the non-resonant energy transfer from the $^2F_{5/2}$ level (Yb^{3+}). Two emission bands are observed from the $^1G_4$ level, first associated with the $^1G_4 \rightarrow {}^3H_6$ transition at 473 nm and second associated with the $^1G_4 \rightarrow {}^3F_4$ transition at 647 nm. Cooperative sensitization up-conversion is

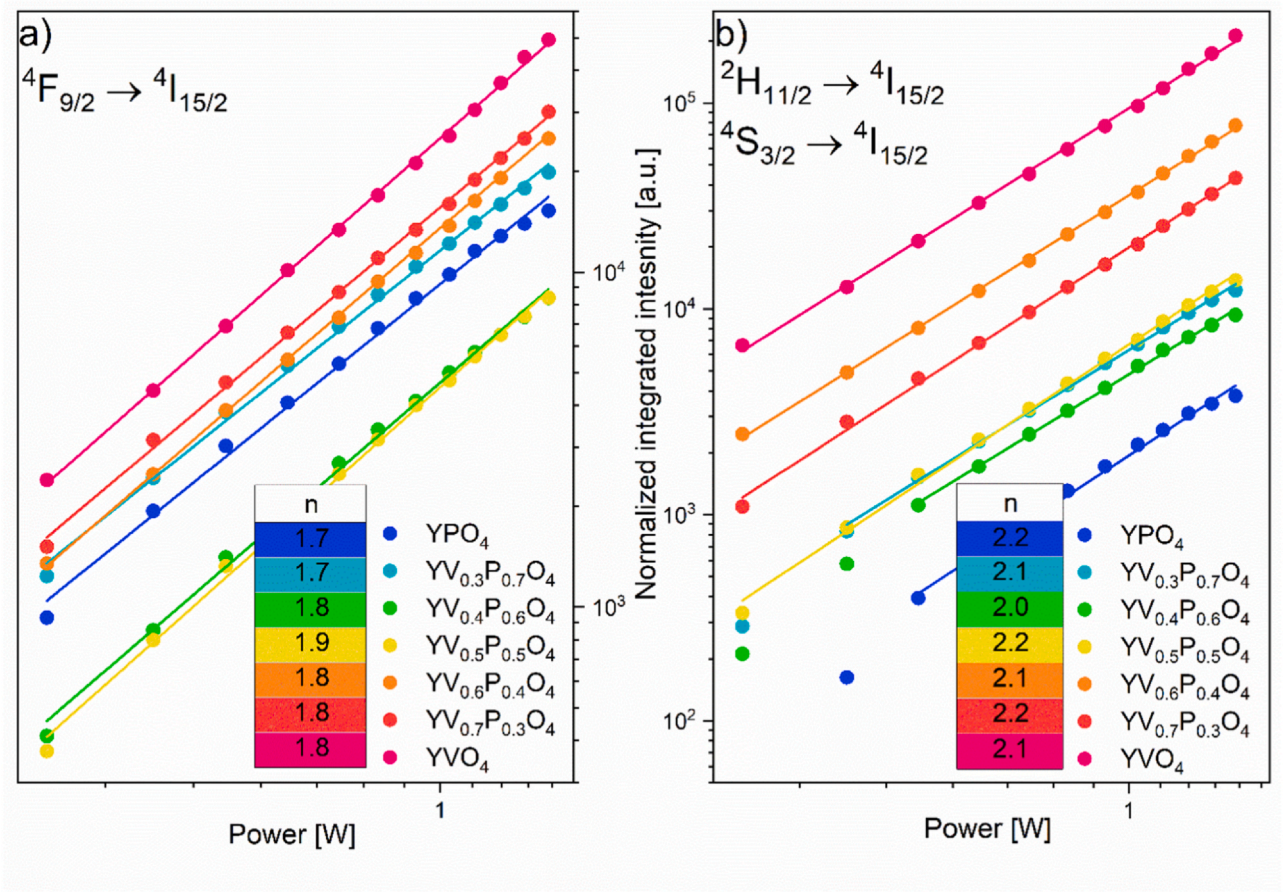

Fig. 9. Double logarithmic dependence of the emission intensity on the laser pump power of the $^4F_{9/2} \rightarrow {}^4I_{15/2}$ transition (a) and the $^2H_{11/2} \rightarrow {}^4I_{15/2}$, $^4S_{3/2} \rightarrow {}^4I_{15/2}$ transitions (b) in 1 mol% Er^{3+}, 20 mol% Yb^{3+}:$YV_xP_{1-x}O_4$ measured with FESH0850 filter at 300 K.

marked with pink, dashed, bended arrows, showing energy transfer from two separate Yb^{3+} sensitizer centers. Possible pathway for the $^1G_4$ level population is via cooperative sensitization process, which relies on direct and simultaneous energy transfer from two Yb^{3+} ions excited to the $^2F_{5/2}$ level. Therefore, population of the $^1G_4$ level can originate from subsequent absorption of two photons. Cooperative sensitization between Yb^{3+}-Yb^{3+} → Tm^{3+} has been proposed to be responsible for the population of the $^1G_4$ level [25,26,30].

Within materials co-doped with 1 mol% Er^{3+} and 20 mol% Yb^{3+} the process proceeding the ETU and ESA is Ground State Absorption (GSA), marked with black, solid arrow in the Fig. 12**.** Excited State Absorption (ESA) is marked with orange, dashed arrow and occurs within erbium ions causing excitation of the higher states (i.e., $^4F_{7/2}$) from the first excited state ($^4I_{11/2}$). In erbium-ytterbium co-doped materials, population of the Er^{3+} upper levels is more complex, than in case of Tm^{3+}, and involves: energy transfer up-conversion (black, dashed, bended arrows), excited state absorption (orange, dashed arrow) and cross-relaxation (yellow, dotted arrows). The preceding process for excited state absorption is ground state absorption (black, solid arrow), which leads to populating the $^4I_{15/2}$ level. Excitation to the upper $^4F_{7/2}$ level within Er^{3+} ion is caused by the absorption of subsequent photon. Further, the $^4F_{7/2}$ level is depopulated via non-radiative relaxation to the $^2H_{11/2}$ level, emission to the ground state may be observed at 523 nm or non-radiative relaxation of the $^2H_{11/2}$ level may lead to populating next lower lying the $^4S_{3/2}$ level. The $^4S_{3/2} \rightarrow {}^4I_{15/2}$ transition is associated with emission at 547 nm. The $^4F_{9/2}$ level is populated by the cross-relaxation processes (yellow, dashed arrows) between two erbium ions [31]. Cross-relaxation is a process of non-radiative energy transfer between two adjacent ions of the same element (herein Er^{3+}). One ion lowers its excitation energy by depopulating to a lower excited state, this energy is transferred to other ion leading to population of its higher states. In the scheme marked with yellow, dotted arrows. The cross-relaxation process causes quenching the luminescence of one kind of ions [32]. Energy transfer related to up-conversion in Er^{3+}-Yb^{3+} (black, dashed, bended arrows) pairs is involving a non-resonant energy transfer from excited sensitizer center (the $^2F_{5/2}$ level of Yb^{3+}) to the $^4I_{11/2}$ level in Er^{3+}. Second non-resonant energy transfer from the $^2F_{5/2}$ level (Yb^{3+}) is leading to population of the $^4F_{7/2}$ level in Er^{3+} and non-radiative relaxation to the $^2H_{11/2}$ level. Emission to the ground state ($^2H_{11/2} \rightarrow {}^4I_{15/2}$, 523 nm) or non-radiative relaxation may occur and lead to populating the lower lying $^4S_{3/2}$ level and further, radiatively relax to the ground state ($^4S_{3/2} \rightarrow {}^4I_{15/2}$, 547 nm).

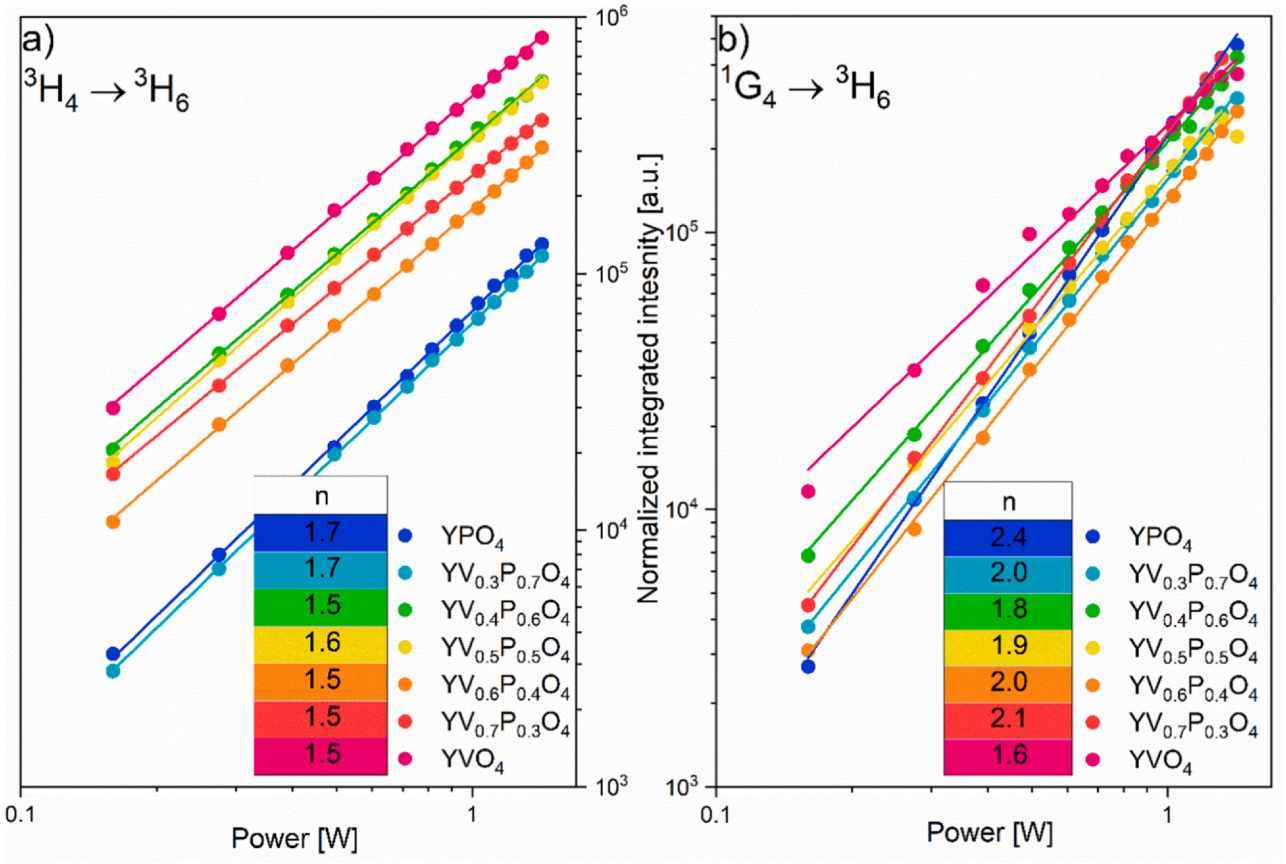

Fig. 10. Double logarithmic dependence of the emission intensity on the laser pump power of the $^3H_4 \rightarrow {}^3H_6$ transition (a) measured with Schott KG5 filter and of the $^1G_4 \rightarrow {}^3H_6$ transition (b) measured with filter FESH0850 in 0.25 mol% Tm^{3+}, 20 mol% Yb^{3+}:$YV_xP_{1-x}O_4$ (300 K).

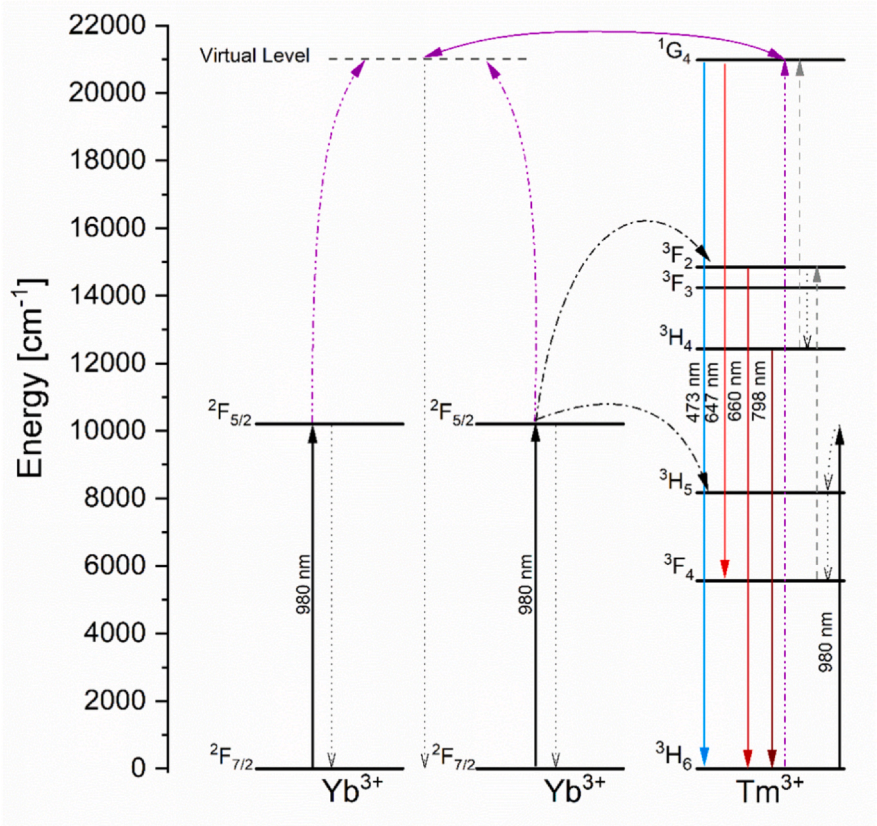

Fig. 11. Energy level scheme with proposed up-conversion processes occurring in 0.25 mol% Tm^{3+}, 20 mol% Yb^{3+}:$YV_xP_{1-x}O_4$.

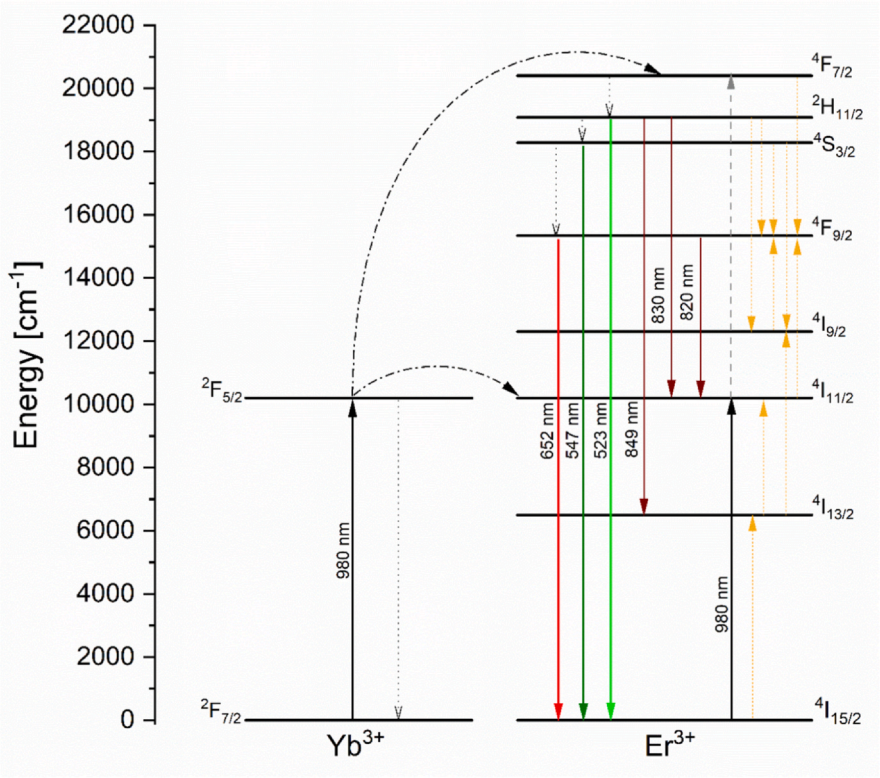

Fig. 12. Energy level scheme with proposed up-conversion processes occurring in 1 mol% Er^{3+}, 20 mol% Yb^{3+}:$YV_xP_{1-x}O_4$.

4. Conclusion

The thulium-ytterbium and erbium-ytterbium co-doped yttrium orthovanadate-phosphate system ($YV_xP_{1-x}O_4$, $0 \le x \le 1$) has been synthesized via co-precipitation method. Applied synthesis route leads to obtaining pure tetragonal nanocrystals. Analysis of yttrium orthovanadate-phosphate system's crystal phase purity, morphology as well as spectroscopic properties were studied extensively. The regularity in spectroscopic and structural properties of solid solutions ($YV_xP_{1-x}O_4$) associated with changing vanadium concentration has been described in detail. An influence of vanadium(V) concentration on up-conversion processes was characterized by performed measurements.

Declaration of Competing Interest

The authors declare that they have no known competing financial interests or personal relationships that could have appeared to influence the work reported in this paper.

Acknowledgment

The authors would like to thank E. Bukowska for performing XRD measurements, D. Szymański for SEM images and the National Science Centre in Poland (NCN - Narodowe Centrum Nauki) for the financial support within the Project „*Preparation and modulation of spectroscopic properties of YXZO4, where X and Z - P^{5+}, V^{5+}, As^{5+}, doped with 's^2-like' ions and co-doped with rare earth ions*" (No. UMO-2019/33/B/ST5/02247).

References

[1] M. Runowski, A. Shyichuk, A. Tymiński, T. Grzyb, V. Lavin, S. Lis, Multifunctional optical sensors for nanomanometry and nanothermometry: high-pressure and high-temperature upconversion luminescence of lanthanide-doped phosphates - LaPO4 /YPO4:Yb3+ – Tm3+, ACS Appl. Mater. Interface Appl. Mater. Interfaces 10 (2018) 17269–17279, https://doi.org/10.1021/acsami.8b02853

[2] M. Soharab, I. Bhaumik, R. Bhatt, A. Saxena, A.K. Karnal, Effect of Yb co-doping on the spectral properties of Er: YVO4 single crystal: a Judd Ofelt analysis, J. Lumin. 200 (2018) 280–286, https://doi.org/10.1016/j.jlumin.2018.03.050

[3] Y. Cheng, K. Sun, Green, blue, red, near-infrared up-conversion luminescence of Yb3+/Er3+/Tm3+ co-doped YVO4 nanoparticles, J. Nanopart. Res. 20 (2018) 168, https://doi.org/10.1007/s11051-018-4268-5

[4] Y. Cheng, K. Sun, Sol – gel synthesis and upconversion luminescent properties of Yb3+, Er3+, Eu3+ triply-doped in YVO4 phosphors, J. Fluoresc. 28 (2018) 285–291, https://doi.org/10.1007/s10895-017-2191-2

[5] J. Zhang, Y. Wang, Z. Xu, H. Zhang, P. Dong, L. Guo, F. Li, S. Xin, W. Zeng, Preparation and drug-delivery properties of hollow YVO4:Ln3+ and mesoporous YVO4:Ln3+@nSiO2@mSiO2 (Ln ¼ Eu, Yb, Er, and Ho), J. Mater. Chem. B 1 (2013) 330–338, https://doi.org/10.1039/c2tb00045h

[6] G. Dantelle, R. Calderon-Villajos, C. Zaldo, C. Cascales, T. Gacion, Nanoparticulate coatings with efficient up-conversion properties (doi:dx.doi.org/), ACS Appl. Mater. Interfaces 6 (2014) 22483–22489, https://doi.org/10.1021/am5065377

[7] Y. Zhang, Y. Li, P. Li, G. Hong, Y. Yu, Preparation and upconversion luminescence of YVO4: Er3+, Yb3+, Int. J. Miner. Metall. Mater. 17 (2010) 225–228, https://doi.org/10.1007/s12613-010-0218-7

[8] S.K. Omanwar, S.R. Jaiswal, N.S. Sawala, K.A. Koparkar, V.B. Bhatkar, Ultra-violet to visible quantum cutting in YPO4: Gd3+, Tb3+ phosphor via down conversion, Mater. Discov. 7 (2017) 15–20, https://doi.org/10.1016/j.md.2017.05.003

[9] A. Tang, P. Ding, N. Song, S. Tang, L. Shi, Y. Zhao, Silicate micro-spheres modified with YPO4: Pr3+ particles: possessing light diffusion and blue-light down-conversion properties, Mater. Lett. 161 (2015) 395–398, https://doi.org/10.1016/j.matlet.2015.08.152

[10] K.Y. Li, L.Y. Liu, R.Z. Wang, Z. Xiao, H. Yan, Broadband sensitization of down-conversion phosphor YPO4 by optimizing TiO2 substitution in host lattice co-doped with Pr3+-Yb3+ ion-couple, J. Appl. Phys. (2014) 115, https://doi.org/10.1063/1.4869659 123103.

[11] W.O. Milligan, D.F. Mullica, Structural investigations of YPO4, ScPO4, and LuPO4, Inorg. Chem. Acta 60 (1982) 39–43, https://doi.org/10.1016/S0020-1693(00)91148-4

[12] B.C. Chakoumakos, M.M. Abraham, L.A. Boatner, Crystal structure refinements of zircon-type MVO4 (M = Sc, Y, Ce, Pr, Nd, Tb, Ho, Er, Tm, Yb, Lu), J. Solid State Chem. 109 (1994) 197–202, https://doi.org/10.1006/jssc.1994.1091

[13] F. Auzel, Upconversion and anti-stokes processes with f and d ions in solids, Chem. Rev. 104 (2004) 139–173, https://doi.org/10.1021/cr020357g

[14] J.R. Rustad, Density functional calculations of the enthalpies of formation of rare-earth orthophosphates†, Am. Mineral. 97 (2012) 791–799, https://doi.org/10.2138/am.2012.3948

[15] G. Strada, M. Schwendimann, La struttura cristallina di alcuni fosfati ed arseniati di metalii trivalenti. II. Arseniato e fosfato di ittrio, Gazetta Chim. Ital. 64 (1934) 662–674.

[16] R.C. Ropp, B. Carroll, Yttrium phosphate-yttrium vanadate solid solutions and Vegard's law, Inorg. Chem. 14 (1975) 2199–2202, https://doi.org/10.1021/ic50151a034
[17] G. Pan, H. Song, Q. Dai, R. Qin, X. Bai, B. Dong, L. Fan, F. Wang, Microstructure and optical properties of Eu3+ activated YV 1-xPxO4 phosphors, J. Appl. Phys. (2018) 104, https://doi.org/10.1063/1.3003130
[18] V. Biju, N. Sugathan, V. Vrinda, S.L. Salini, Estimation of lattice strain in nanocrystalline silver from X-ray diffraction line broadening, J. Mater. Sci. 43 (2008) 1175–1179, https://doi.org/10.1007/s10853-007-2300-8
[19] J. Eckert, J. Holzer, C. Krill, W. Johnson, Reversible grain size changes in ball-milled nanocrystalline Fe–Cu alloys, J. Mater. Res. 7 (1992) 1980–1983, https://doi.org/10.1557/JMR.1992.1980
[20] A.A. Nazarov, A.E. Romanov, R.Z. Valiev, On the nature of high internal stresses in ultrafine grained materials, Nanostruct. Mater. 4 (1994) 93–101, https://doi.org/10.1016/0965-9773(94)90131-7
[21] W. Qin, J.A. Szpunar, Origin of lattice strain in nanocrystalline materials, Philos. Mag. Lett. 85 (2005) 649–656, https://doi.org/10.1080/09500830500474339
[22] H.D. Nguyen, S. il Mho, I.H. Yeo, Preparation and characterization of nanosized (Y,Bi)VO4:Eu3+ and Y(V,P)O4:Eu3+ red phosphors, J. Lumin. (2009) 1754–1758, https://doi.org/10.1016/j.jlumin.2009.04.054
[23] M. Pollnau, D.R. Gamelin, S.R. Lüthi, H.U. Güdel, M.P. Hehlen, Power dependence of upconversion luminescence in lanthanide and transition-metal-ion systems, Phys. Rev. B 61 (2000) 3337–3346, https://doi.org/10.1103/PhysRevB.61.3337
[24] X. Wang, Q. Zhu, J.G. Li, Z. Hu, G. Zhu, C. Wang, La2O2S:Tm/Yb as a novel phosphor for highly pure near-infrared upconversion luminescence, Scr. Mater. 149 (2018) 121–124, https://doi.org/10.1016/j.scriptamat.2018.02.031
[25] A.K. Soni, V.K. Rai, Intrinsic optical bistability and frequency upconversion in Tm3+-Yb3+ - codoped Y2WO6 phosphor, Dalt. Trans. 43 (2014) 13563–13570, https://doi.org/10.1039/c4dt01266f
[26] X. Pei, Y. Hou, S. Zhao, Z. Xu, F. Teng, Frequency upconversion of Tm3+ and Yb3+ codoped YLiF4 synthesized by hydrothermal method, Mater. Chem. Phys. 90 (2005) 270–274, https://doi.org/10.1016/j.matchemphys.2004.03.013
[27] X.B. Chen, W.M. Du, N. Sawanobori, G.Y. Zhang, Z.F. Song, Initial experimental comparative investigation of direct and indirect up-conversion sensitization of the 1G4 level of Tm, Yb co-doped material, Opt. Commun. 181 (2000) 171–181, https://doi.org/10.1016/S0030-4018(00)00636-2
[28] L. Shi, C. Li, Q. Shen, Z. Qiu, White upconversion emission in Er3+/Yb3+/Tm3+codoped LiTaO3 polycrystals, J. Alloys Compd. 591 (2014) 105–109, https://doi.org/10.1016/j.jallcom.2013.12.234
[29] G.Y. Chen, Y. Liu, Y.G. Zhang, G. Somesfalean, Z.G. Zhang, Q. Sun, F.P. Wang, Bright white upconversion luminescence in rare-earth-ion-doped Y2O3 nanocrystals, Appl. Phys. Lett. 91 (2007) 1–4, https://doi.org/10.1063/1.2787893
[30] L. Li, H. Lin, X. Zhao, Y. Wang, X. Zhou, C. Ma, X. Wei, Effect of Yb3+ concentration on upconversion luminescence in Yb3+, Tm3+ co-doped Lu2O3 nanophosphors, J. Alloys Compd. 586 (2014) 555–560, https://doi.org/10.1016/j.jallcom.2013.10.122
[31] W. Wei, Y. Zhang, R. Chen, J. Goggi, N. Ren, L. Huang, K.K. Bhakoo, H. Sun, T.T.Y. Tan, Cross relaxation induced pure red upconversion in activator-and sensitizer-rich lanthanide nanoparticles, Chem. Mater. 26 (2014) 5183–5186, https://doi.org/10.1021/cm5022382
[32] G.G. Demirkhanyan, R.B. Kostanyan, F.P. Safaryan, T.V. Sanamyan, Cross-relaxation processes from the 4S3/2 level of the Er 3+ ion in Lu3Als012, Plenum Publ. Corp. 48 (1988) 1987–1989.